TRANSIENT AND IMPACT DYNAMICS OF A MICRO-ACCELEROMETER

G. Li*
OMM Inc.
San Diego, California 92121 USA
E-mail: gli@omminc.com

and

A. A. Tseng
Department of Mechanical and Aerospace Engineering
Arizona State University
Tempe, Arizona 85287-6106 USA
E-mail: ampere.tseng@asu.edu; Fax: (480) 965-1384

ABSTRACT

The transducer of a micro-machined accelerometer is designed to function in a moving environment which is either accelerating, decelerating or oscillating. To ensure short-term functionality and long-term reliability, the design of a particular motion sensing transducer requires both static and dynamic analyses. In this paper, dynamic analysis has been performed for the transducer structure of a micro-accelerometer system. The external load is acceleration. Both displacement and stress are closely examined under various levels of applied acceleration. The influence of damping and residual film stress are determined. Finally, the consequence of impact is investigated and an experimental test of the electrical latch is presented. A theoretical analysis is carried out to explain when a latch may occur and how to prevent it from occurring.

---

* Formerly with Motorola Inc., Mesa, Arizona.
in J. Mat. Processing & Manufacturing Science Vol. 9, No. 2, pp. 143-156, 2000.

1. INTRODUCTION

An important component of engineering design is the analysis and prediction of the dynamic behavior of physical systems. An accelerometer is a prime example of such a system, designed specifically to measure shock and vibration. Understanding the limitations of the system helps to ensure repeatable and reliable performance. This is of particular importance when measuring acceleration for safety applications such as air bag deployment. Dynamic analyses for vibrations with amplitudes up to 2000 g are presented for a surface micromachined microelectromechanical transducer designed to measure moderate accelerations up to 100 g (Ristic et. al., 1992).

Following an introduction, this paper will begin by discussing the composition of the transducer and how it is modeled by the technique of finite element analysis (FEA). Model validation, namely comparing and correlating simulation data with the corresponding experimental observations is also described. Simulation data of dynamic analysis, in which both displacements and stresses are calculated in the time domain, is then presented. Finally, the dynamic behavior of the accelerometer under impact is studied.

The results indicate that, regardless of the magnitude of the applied acceleration, the maximum dynamic stress is saturated to about 10 MPa. In addition, a different dynamic behavior caused by impact (i.e. electrical latching of the sensor's moving component) will also be discussed. A latch mathematical model is presented, and a family of latch criteria is obtained for the transducer under consideration.

2. FEA MODELING AND MODEL VALIDATION

A micro-accelerometer developed and fabricated by Motorola is studied (Schemansky et. al., 1995); it is basically comprised of three components: a bottom polysilicon layer adhering to the substrate, a top polysilicon layer anchored at various points also to the substrate, and a middle layer of polysilicon suspended by four tether beams to the substrate. The middle layer with the top and bottom layers respectively form two capacitors. When subjected to an inertial force, the middle layer is deflected, either toward the top or the bottom layer depending on the direction of the inertial force. This motion in turn results in changes in capacitance for both capacitors generating a differential output signal. A SEM micrograph of this capacitive device is shown in Figure 1.

Mechanically, both the bottom and top polysilicon layers have little motion relative to the substrate, and together with the substrate they may be considered as rigid bodies. The focal point is the middle movable layer, in this case an octagonal plate with four tethers anchored to the substrate. The plate serves as the "proof mass" for the accelerometer, and contains 52 smaller holes spread over the plate and a larger hole in the center. The smaller holes were introduced for two reasons: 1) to allow easier removal of the sacrificial oxide layers during fabrication, and 2) to control damping. The larger central hole is used to provide an additional anchor from the top layer to the substrate (Fig. 1).

The four tether suspension beams are made of polysilicon and silicon nitride layers. A thin layer of silicon nitride is sandwiched by two polysilicon layers. Experiments show that the silicon

nitride layer fabricated by low-pressure chemical vapor deposition (LPCVD) at temperature of 800°C exhibits a tensile stress of approximately 1100 MPa. The doped polysilicon, also fabricated by LPCVD at a lower temperature of 600 °C, is compressive in the neighborhood of 22 MPa.

The combination of both nitride and polysilicon stresses is still tensile along the tether, and therefore it is able to suspend the central plate. In FEA modeling, the residual stress is typically specified indirectly by introducing artificial thermal expansion coefficients and/or thermal loads. If a 22 MPa compressive stress is desired for polysilicon and 1100 MPa for nitride, a temperature increase of 1 °C can be assumed and two fictitious thermal expansion coefficients can be computed in the following manner:

$$\alpha_p = 22 / E_p, \qquad \alpha_n = -1100/E_n, \tag{1}$$

where E_p and E_n are Young's moduli for nitride and poly, respectively. Based on literature values (Peterson, 1982), E_p and E_n are equal to 385 x 10^3 MPa and 160 x 10^3 MPa, respectively. It is important to be clear that both polysilicon and nitride stresses vary from wafer to wafer. Adjustments may be necessary to correlate simulation with experimental data. It should also be made clear that the holes in the movable polysilicon layer were not directly included in our FEA modeling and their effects were taken into account by employing a smaller mass density for the octagonal plate and using a damping coefficient directly measured from real devices.

The finite element results of the residual stresses introduced during fabrication or by the artificial thermal expansion coefficients are shown in Figure 2. It is obvious that the stress in the central plate is minimal, while the tether beams carry significant stress. The greatest stress concentrations occur near the tether-plate joints and at the anchor points. As shown by the legends

on the right margin in the figure, the maximum stress is 629 MPa. It should be noted that due to relatively coarse meshing, high stresses are not caused by sharp corners at these locations. In practice, stress concentration is minimized by adding the proper fillet. Figure 2 also shows deformation of the structure induced by the residual film stresses in both polysilicon and nitride. The maximum stress-induced displacement occurs at the center with a numerical value of 0.106 μm. In comparison, it was found that the average residual stress-induced displacement in actual devices was approximately 0.1 μm. In this regard, the numerical result from the FEA model correlates well with the test data. A scale factor of 200 was used in the figure to clearly show the resulted deformation. Since no external load is involved, the results shown in Fig. 2 can also be served as a baseline or reference for later assessment of the dynamic effects under acceleration loading.

An alternative and independent model validation was also carried out by computing the system's natural frequency characteristics and comparing it with the experimental data. The experimental data was obtained by mounting an accelerometer to an electric shaker and measuring the system response in a frequency range from 0 to 25 kHz. The input load from the shaker was acceleration and was kept to a constant. In the numerical simulation, a damping ratio of 0.53, which was directly extracted from experimental data, was used.

Figure 3 shows both experimental (circles) and numerical data (solid line). An excellent agreement between the data is clearly observed. The data was normalized by converting the numerical result into the same format as the experimental data such that the amplitude of the system response at low frequency, near zero, is unity. Once the FEA model has been established

and validated, it is possible to employ the model to predict the dynamic behavior of the transducer under a variety of operating and environmental conditions.

3. TRANSIENT DYNAMICS

Static analysis is important in evaluating a sensor structure and in setting operating limits. Transient dynamic analysis also plays an important role in the overall design by helping refine limitations set by static analysis and producing information on fatigue life and long term reliability. The objective of this section is to present simulation results of the transducer in a time domain and to determine the effects of variations of system damping and residual film stress.

3.1 Equivalent Stress

For the transducer structure, the stress near the anchors and the joints, where the tether arms connect to the proof-mass, is rather complex and is high in magnitude. All six independent stress components are generally present at each material point. In such a situation, an equivalent stress proposed by Von Mises is often used as a single representation to reflect the stress magnitude and to compare it against commonly accepted stress criteria for design purposes. Let (σ_x, σ_y, σ_z, τ_{xy}, τ_{yz}, τ_{zx}) be the independent stress components, the equivalent stress (also known as Von Mises stress) is defined as (Owen and Hinton, 1980):

$$\sigma_e = \frac{1}{\sqrt{2}}\left\{(\sigma_x - \sigma_y)^2 + (\sigma_y - \sigma_z)^2 + (\sigma_z - \sigma_x)^2 + 6(T_{xy} + T_{yz} + T_{zx})^2\right\}^{\frac{1}{2}} \quad . \qquad (2)$$

In the case of a uni-axial stress, where all stress components are zero except σ_x, we have:

$$\sigma_e = |\sigma_x| \qquad (3)$$

Notice that by definition, σ_e is always positive.

3.2 Damping Effects

Damping is of great interest in designing a movable mechanical system. Minimal damping may result in large vibrations upon excitation. On the other hand, over damping may result in a reduced signal and a sluggish response. It is important to examine the system dynamic behavior and its dependence on damping for the optimal design.

For the transducer system, the damping ratio could vary within the range of 0.1 to 5 depending on the packaging pressure. Roughly, if the device is packaged at 20 Torr, it has a damping ratio in the neighborhood of 1.0 (critically damped). Reducing the packaging pressure to about 2 Torr will result in a smaller damping of approximately 0.1. By setting all system parameters to their default values, and running the simulation for damping ratios at 0.1, 0.5 and 1.0, both displacements and stresses can be calculated. Figure 4 shows the stress variation (equivalent stress) in the time domain for a material point near one of the joints where thethe tether is connected to the octagon and the stress is maximum. The applied acceleration is 50 g. The three curves are for different damping ratios of 0.1 (solid), 0.5 (dotted) and 1.0 (dashed). At a damping of 1.0, the structure is no longer oscillating and is slowly converging to its equilibrium position. The final steady state, as $t \to +\infty$, does not depend on damping.

It should be emphasized that the stress as shown in Figure 4 is purely due to the application of acceleration and is referred to as *dynamic stress*. The total structural stress is the summation of the initial residual stress and the dynamic stress. Note that compared to the initial residual stresses (approximately 20 MPa compressive in polysilicon and 1100 MPa tensile in nitride), the dynamic stress (0.5 MPa) under 50 g is relatively small. The combined stress (static + dynamic) is still far

below the endurance limit of both polysilicon and silicon nitride and is not of major concern regarding fatigue life and structural integrity. It is to be noted that rupture stress for polysilicon material is difficult to find from published literature. However, it is expected that this critical stress is higher than the rupture stress for a single crystal silicon for which large amounts of research has been done. According to the data in Huff et. al. [1993], the rupture stress for polysilicon is somewhere from 600 to 1200 MPa.

3.3 Residual Film Stress Effects

Residual film stress is also a concern in MEMS designs since it impacts the system response. It is known that the processing tolerances for micromachining have distinct and finite limitations, and that, very often, the geometric dimensions and film stresses may significantly deviate from their respective designed values. Therefore, it is necessary to evaluate the system response and sensitivity to these deviations. In this subsection, simulation results are again presented, but this time, with the residual polysilicon stress as a primary parameter. Specifically, three polysilicon stresses at 15, 20, and 25 MPa are considered. The tensile nitride stress is fixed at 1100 MPa.

Once again, the displacements and stresses of the movable layer with three-levels of residual polysilicon stresses is calculated. The stresses near a joint where the stress is maximum are shown in Figure 5. A trend is clear: as the polysilicon stress is increased from 15 to 25 MPa, both the amplitude of oscillation and the resulting dynamic stress become larger. This can be explained by the fact that since polysilicon stress is compressive, a larger compressive stress reduces the structural rigidity thus resulting in a larger deflection and larger dynamic stress under

the same loading condition. In the extreme, as the compressive stress becomes equal or larger than the buckling stress for the structure, the structural rigidity would vanish and the structure may collapse under arbitrarily small perturbations.

4. IMPACT DYNAMICS AND LATCH PHENOMENON

In design of the micro-accelerometer, the dynamic analysis of transducer structure is required to ensure its long-term reliability. In this section, the dynamic analysis of the micro-accelerometer structure under external acceleration loading is described. The resulted electrical latch phenomenon is also presented.

4.1 Impact Under High 'g'

One method of assessing reliability and fatigue life of a MEMS acceleration sensor is to test the device under an artificially high 'g'. Typically, a 500 g powered test and a 2000-g power-off test are required. Mechanically, the magnitude of displacement and stress of the structure should be determined under these high 'g' loads. In short, it should be ascertained that the dynamic stress is small enough to allow adequate fatigue life and that the structure is not pushed beyond (or even close to) a stress level at which rupture or other types of damage may occur. After experiencing a high 'g' input, the structure should return to its normal working conditions without outside intervention.

For the transducer structures under consideration there are four pairs of mechanical stops, which limit the deflection of the middle movable layer. The designed clearance between each pair of polysilicon layers is 1.6 μm (= d_0) and the stop clearance is 1 μm (= d_s). Therefore, although the central plate can move up to 1.6 μm, the motion is limited to 1 μm at the stops. See Figure 6 for a schematic illustration of the mechanical stops.

To simulate the worst possible conditions, acceleration inputs of 500 g, 1000 g, and 2000 g were first applied to the substrate in the positive *z*-direction at t = 0 and then direction was reversed toward the negative z-axis at t = 40 µs. Figure 7 shows displacement curves at both the transducer center (Fig. 7a) and near a joint (Fig. 7b) where a mechanical stop was placed. A damping ratio of 0.1 was used in the simulation. It can be seen that under 500 g, both displacements are less than 1 µm in magnitude. No impact with the stops occurs at all. Under 1000 g, one impact occurs during the second period from 55 to 60 µs as shown in Fig. 7b. Notice that although the displacement at the joint was constrained to 1 µm, the displacement at the center continued to deflect to 1.31 µm at t = 57 µs (Fig. 7a). Under 2000 g, many impacts have occurred as seen in Fig. 7b. Because of the high magnitude of 'g', the movable layer deflects much more at the transducer center and reaches 1.6 µm at t = 57.5 µs (Fig. 7a).

The stresses for the above conditions are plotted in Figure 8. The solid line represents stress for acceleration at 500 g, note that the contour of the line is smooth; the turning point at t = 48 µs results from the definition of the equivalent stress which is always positive regardless of the sign of the actual stress. At 1000 g, represented by the dotted line, the curve is smooth for t < 48 µs, and large fluctuations occur as soon as the structure impacts on the stops. The magnitude of stress is approximately 10 MPa, a stress magnitude large enough to influence the system response yet still too small to cause any damage in terms of fatigue and reliability. At 2000g, the stress (dashed curve) fluctuates even more violently due to impacts. Yet, the overall stress magnitude is still approximately at the same level as for the case of 1000g. In fact, regardless of how high the applied acceleration is, the vibration magnitude is limited by the stops and possibly by the top and

bottom polysilicon layers. Thus, the maximum dynamic stress is somewhat saturated at 10 MPa or slightly higher. No fatigue and reliability problems are anticipated.

4.2 Electrical Latching

Another consequence of impact, which is usually caused by high 'g', is to cause latching of the movable component to the surrounding stationary parts. A centrifuge table is used to evaluate the latching behavior. The centrifuge table is actually a turning table that rotates at a controlled speed. When an accelerometer sample is mounted at a given location on the centrifuge table surface, with the octagon surface pointing to the center, acceleration is generated and applied to the accelerometer. The magnitude of the acceleration (a) equals $R \times \omega^2$, where R is the radius and ω is the angular velocity. As a result, the magnitude of acceleration can be adjusted by changing the angular velocity.

Figure 9 shows the results of two separate experimental tests of an early accelerometer sample. The accelerometer was fixed at a distance from the center of a centrifuge turning table, and acceleration was applied by controlling the angular velocity of the table. Typically, each run was performed by slowly increasing the acceleration up to 200 g and then slowly decreasing the 'g' level back to zero. Normally, the operating voltage is a constant voltage supplied to the accelerometer. The output signal from the accelerometer is also voltage and can be simply measured by a voltemeter. At zero input where there is no acceleration, the output voltage is 2.5 volt.

When the accelerometer tested is powered at 5 volts, which is the designed operating voltage, the movable polysilicon layer starts contacting the mechanical stop at approximately 125 g. Thereafter, the output voltage is flat, since the movable polysilicon plate is constrained by the mechanical stop and remains virtually stationary. When the applied acceleration was gradually released, the movable polysilicon plate began leaving the mechanical stop, also at about 125 g, and returned to its original position at zero 'g'. This process is clearly shown by curves marked with circles for increasing 'g' and squares for decreasing 'g'. There was no electrical latch-up.

For demonstration purposes, the same accelerometer was tested again with a higher applied voltage of 7 volts. In this run, the movable polysilicon plate starts contacting the mechanical stop at a much lower 'g' because of a much larger electrical force. Even after the applied acceleration was reduced to zero, the movable polysilicon plate failed to retrieve as shown by the flat curve marked with crosses. The movable layer is latched to the mechanical stop by electrical force. The electrical force between poly1 and poly2 and between poly2 and poly3 can be found to be proportional to the square of an applied voltage: $F = \zeta AV^2/(2d)$, where ζ is the dielectric constant equal to 8.85×10^{-12} F/m at air, A is the area, V is the applied voltage, and d is the gap between the two polysilicon layers involved.

4.3 Latching Analysis

In this section, a simplified mathematical model of the transducer is presented to explain the latch phenomenon. Such an analysis helps to design a better transducer with improved performance.

Considering the movable polysilicon plate (poly-2) as a rigid body supported by springs as shown in Figure 6, its motion can be described by a second order ordinary differential equation as follows (Meirovitch, 1975):

$$m\ddot{x} + c\dot{x} + kx = \frac{\varepsilon_0 A V^2}{2}\left\{\frac{1}{(d_0 - x)^2} - \frac{1}{(d_0 + x)^2}\right\} + ma\sin \omega t, \qquad (4)$$

where m is the mass of the movable polysilicon plate; c is the damping coefficient of air; k is the spring constant of the supporting tethers; ε_0 is the permittivity constant; A is the area of the movable polysilicon plate; V is the applied voltage between poly-1 and poly-2 and between poly-2 and poly-3; d_0 is the initial air gap between different polysilicon layers; a is the amplitude of applied acceleration; ω is the angular frequency of applied acceleration; and x is the vertical travel of the movable polysilicon plate.

Upon an impact of the movable polysilicon plate with either the upper or the lower mechanical stop, the movable plate reverses its direction with a slightly reduced speed due to the impact energy loss. Mathematically, this can be expressed as:

$$\dot{x} \leftarrow -r\dot{x} \quad \text{at} \quad x = \pm d_s, \qquad (5)$$

where r is a restitution coefficient, and a numerical value of r = 0.9 will be used in the following simulation and analysis. It is to be noted that upon impact, there is an instant velocity change in both magnitude and direction. The restitution coefficient r is used to reflect the magnitude change. In simulation, a logic command was used to detect an impact. When this occurs, the after-impact velocity is replaced by a smaller velocity and a minus sign is inserted.

The left-hand side of Eq. (4) is simply a representation of a harmonic oscillator with kx as a restoring mechanical force. The first term on the right hand side is a repelling electrical force, and the second term is an oscillatory applied inertial force. Electrical latch occurs when the repelling electrical force is too large or, equivalently, when the mechanical restoring force is too small. To prevent such a latch from happening, the mechanical force must be sufficiently large to overcome the combined electrical forces at the latched positions. Mathematically, this requirement may be expressed as:

$$kd_s \geq \frac{\boldsymbol{e}_0 AV^2}{2}\left[\frac{1}{(d_0 - d_s)^2} - \frac{1}{(d_0 + d_s)^2}\right], \tag{6}$$

where d_s denotes the clearance between a polysilicon layer and its neighboring stop (see Figure 6).

After some algebra, the above relation reduces to:

$$d_s \leq d_{critical} = \left\{ d\frac{2}{0} - \sqrt{\frac{2\boldsymbol{e}_0 AV_2 d_0}{k}} \right\}^{1/2}. \tag{7}$$

For the sensor structure under consideration, where A = 81,457 μm ^{2}, Eq. (7) is graphically illustrated in Fig. 10. Using the solid curve as an example, where k = 3 N/m, if the clearance between the polysilicon layers d_0 is 1.6 μm, to prevent latch from occurring, the theoretical clearance d_s must be no greater than 0.606 μm.

To demonstrate the correctness of latch criterion, Eq. (7), numerical simulation for the full equations (4 & 5) was performed. At k = 3 N/m and d_0 = 1.6 μm, two values of d_s were chosen, 0.6 and 0.62 μm, which are respectively slightly below and slightly above the critical d_s of 0.606 μm. The excitation amplitude was set at 500 g with a low excitation frequency at 20 Hz. At d_s = 0.6 μm (< $d_{critical}$), there should be no latching according to Eq. (7). This is clearly shown by a

dashed curve in Fig. 11. For the first 4 ms, the movable plate was practically instantly following the driving force and impacting with the stops in both sides. At t = 4 ms, at which the applied ‘g’ was set to zero, the proof-mass was slowly returning to its zero position, as expected. For a slightly larger stop clearance at d_s = 0.62 μm, the simulation was repeated in a similar manner. This time, as shown by a solid curve in Figure 11, the proof-mass adhered to the upper mechanical stop and could not return to its normal operating condition before resetting. Therefore, Eq. (7) can be used in the design process to avoid latching.

CONCLUDING REMARKS

A finite element model has been constructed to analyze the dynamic behavior of a micro-machined accelerometer. The model was validated by comparing the simulated frequency response curve against experimental test data as well as by comparing the residual stress induced warpage against measurement data of the accelerometer at zero external load. The effects of both system damping and residual film stress were then examined. The vibration at different damping showed that the system exhibits a classical dynamic behavior of a single-degree-of-freedom mass-spring-dashpot oscillator. The effect of residual stress in polysilicon has been studied and it showed that a larger compressive stress in polysilicon generated a larger dynamic stress. Nevertheless, under the normal loading condition, i.e., a sudden application of 50 g load, all simulated dynamic stress is no greater than one MPa, a stress level too small to cause any concern.

The present study further examined the accelerometer under high 'g' load, a condition related to shock impact or drop test. The simulation data, as shown in Fig.7, showed that the maximum travel of the proof-mass was limited by the mechanical stops as well as by the stationary plates of the accelerometer structure. The maximum dynamic stress was also limited and was in the neighborhood of 10 MPa. Consequently, no fracture would be induced by the dynamic stress and no fatigue is expected for the system over its entire service life.

Finally, the phenomenon of electrical latch was investigated. A latch criterion was derived by treating the accelerometer system as a single-degree-of-freedom oscillator under both an internal electrical force and an external sinusoidal inertial force. A centrifuge turning table test was also performed to verify the reliability of the latch criterion developed. It was shown that the

latch criterion can accurately predict the electrical latch phenomenon and by properly adjusting the clearance of the mechanical stops, electrical latch can be avoided. In fact, the criterion can also be used in the design process to not only avoid latching but also to improve performance.

ACKNOWLEDGMENTS

The authors gratefully acknowledge the support of this research by Motorola Inc. and the U.S. National Science Foundation under Grant No. DMI-9696062 and DMI-9812984. The authors are also indebted to their colleagues: Z. L. Zhang, F.A. Shemansky, and R. Roop for their constructive discussions and contributions.

REFERENCES

Huff, M.; Nikolich, A. D.; and Schmidt, M. A., 1993, *Design of Sealed Cavity Microstructures Formed by Silicon Wafer Bonding* (Journal of MicroElectroMechanical Systems) **2** 74-81.

Meirovitch, L., 1975, *Elements of Vibration* (McGraw-Hill, New York).

Owen, D. R. J. and Hinton, E., 1980, *Finite Elements in Plasticity* (Pineridge: Swansea, U.K.)

Peterson, K. E., 1982, *Silicon as a Mechanical Material*, (Proceedings of the IEEE) **70** 420-457.

Ristic, Lj.; Gutteridge, R.; Dunn, B.; Mietus, D. and Bennett, P., 1992, *Surface Micromachined Polysilicon Accelerometer*, *Technical Digest* (IEEE Solid State Sensor and Actuator Workshop: Hilton Head, SC) 118-121.

Schemansky, F.; Ristic, Lj.; Koury, D. and Joseph, E., 1995, *A Two-Chip Accelerometer System for Automotive Applications*, (Microsystem Technologies) **1** 121.

FIGURE CAPTIONS

Figure 1 SEM micrograph of a capacitive accelerometer

Figure 2 Deformed stress contour of the sensor movable layer (a scale factor of 200 was used)

Figure 3 Frequency response of transducer under sinusoidal ground acceleration.

Figure 4 Dynamic stress responses under 50 g at different damping.

Figure 5 Effect of residual polysilicon stress on final dynamic stress at small damping

Figure 6 Schematic illustration of three polysilicon-layer transducer.

Figure 7 Transient curves of displacements for the transducer structure under high 'g'

Figure 8 Dynamic stresses under high 'g'.

Figure 9 Latching test of accelerometer under two different operating voltages

Figure 10 Latch criteria for a family of spring constants.

Figure 11 Numerical simulation of latch phenomenon

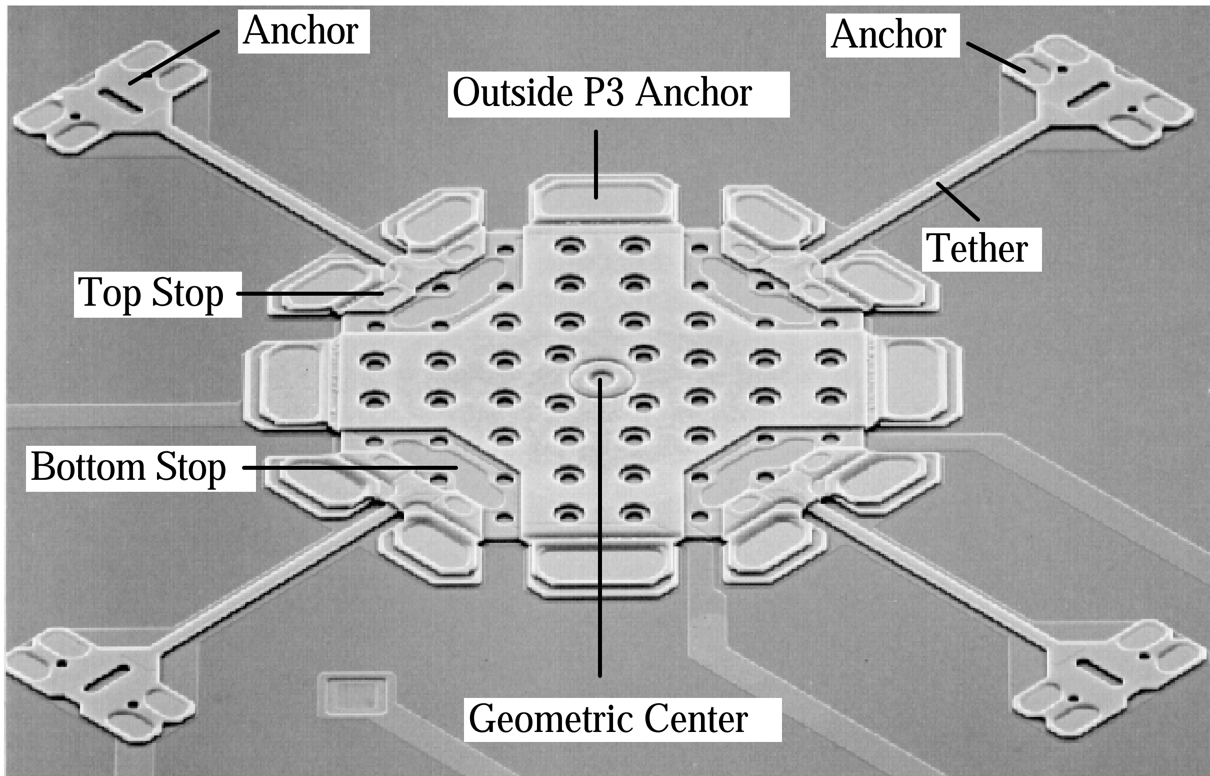

Figure 1 SEM micrograph of a capacitive accelerometer

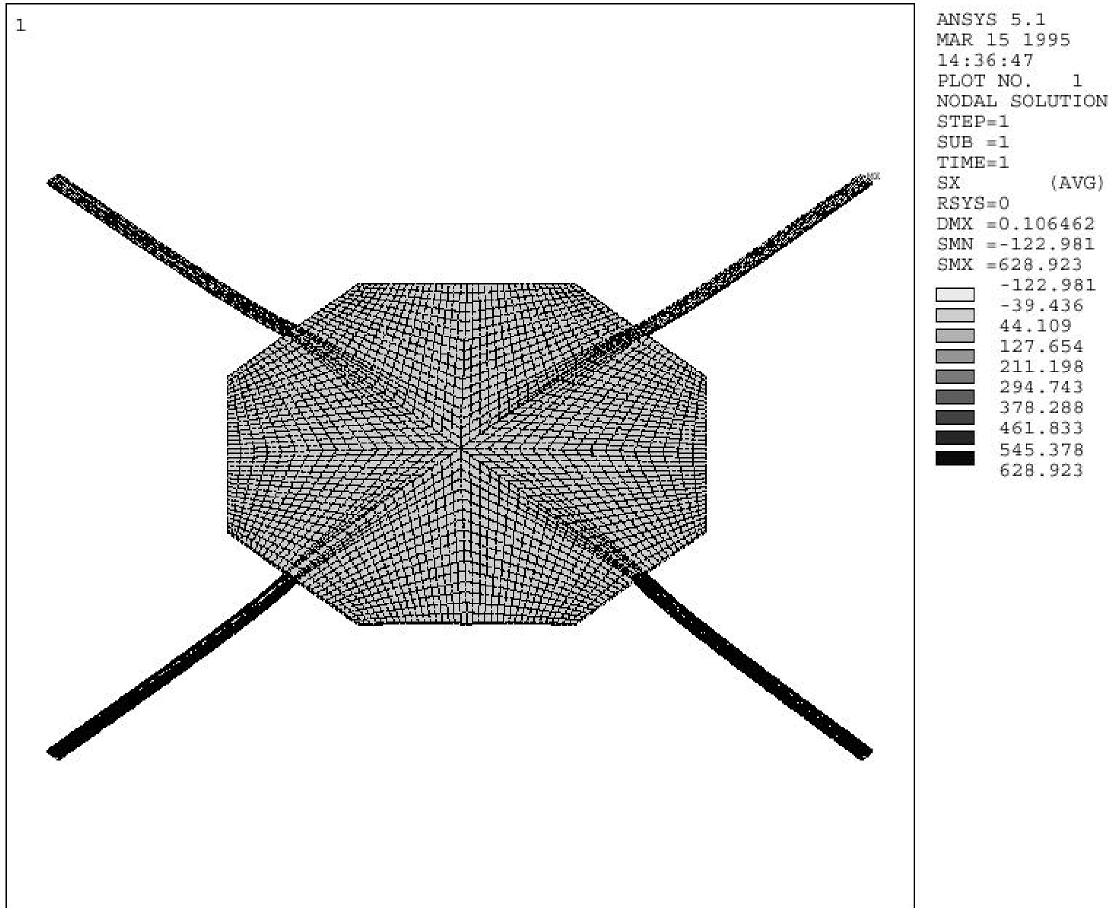

Figure 2 Deformed stress contour of the sensor movable layer
(a scale factor of 200 was used)

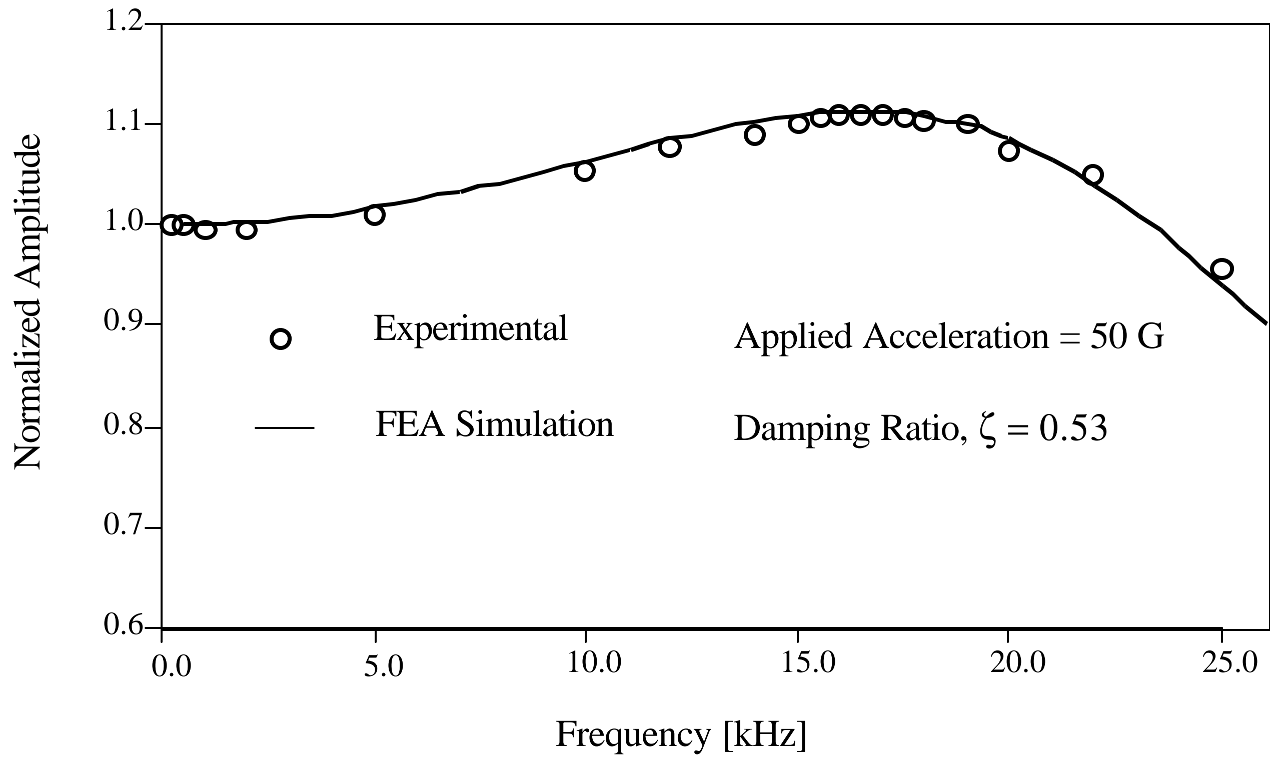

Figure 3 Frequency response of transducer under sinusoidal ground acceleration

.

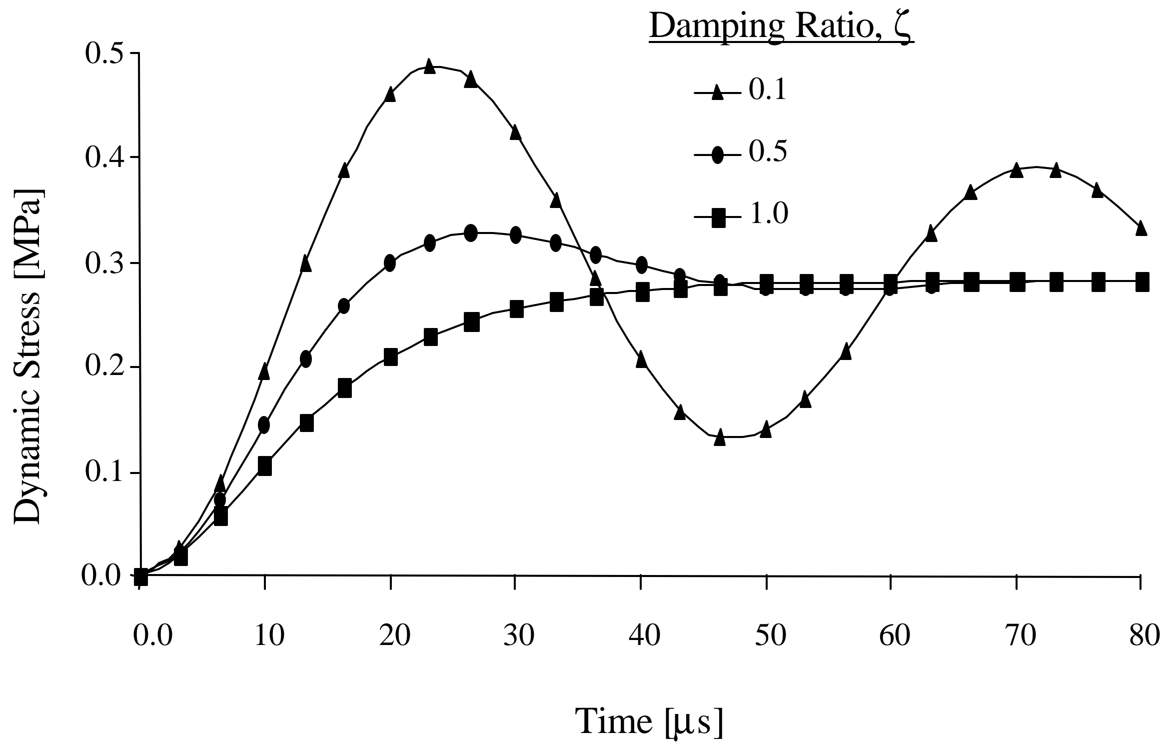

Figure 4 Dynamic stress responses under 50 g at different damping

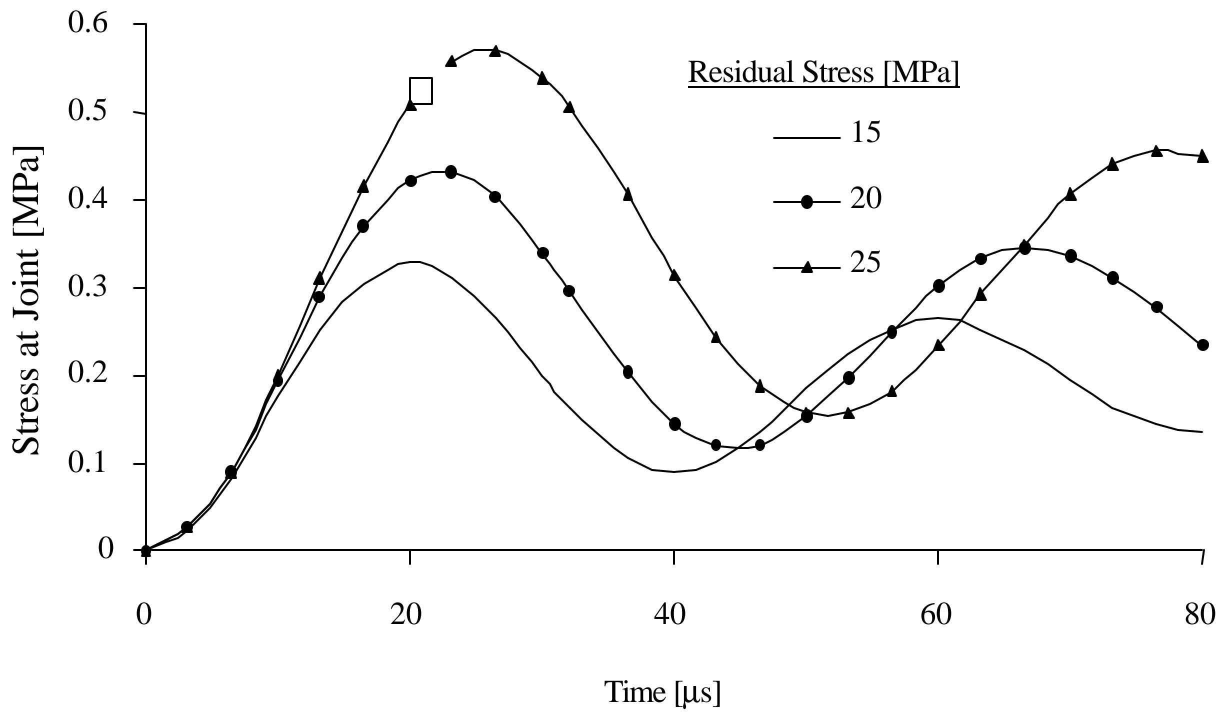

Figure 5 Effect of residual polysilicon stress on final dynamic stress at small damping

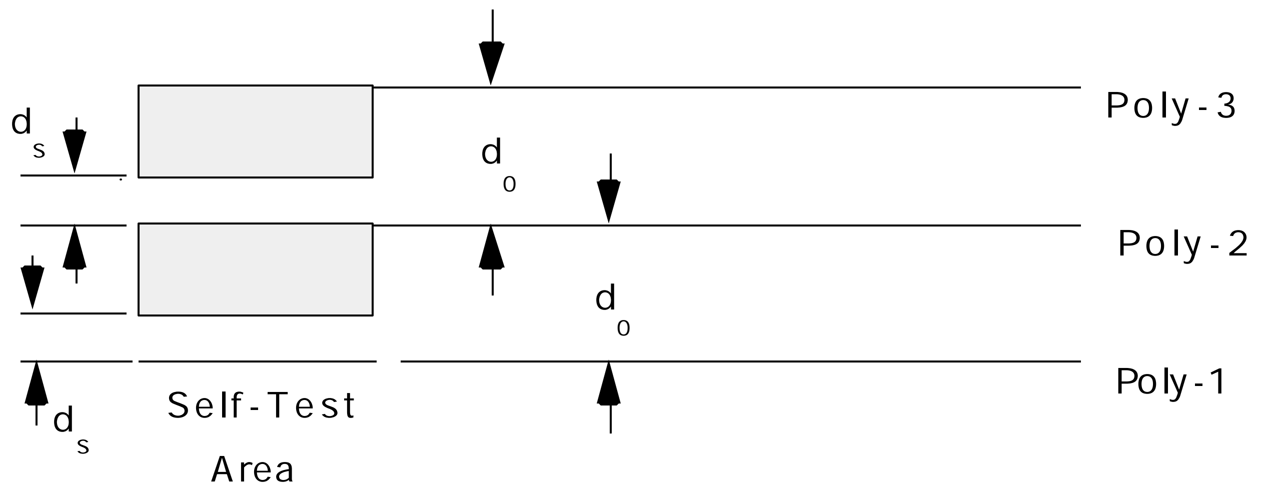

Figure 6 Schematic illustration of three polysilicon-layer transducer

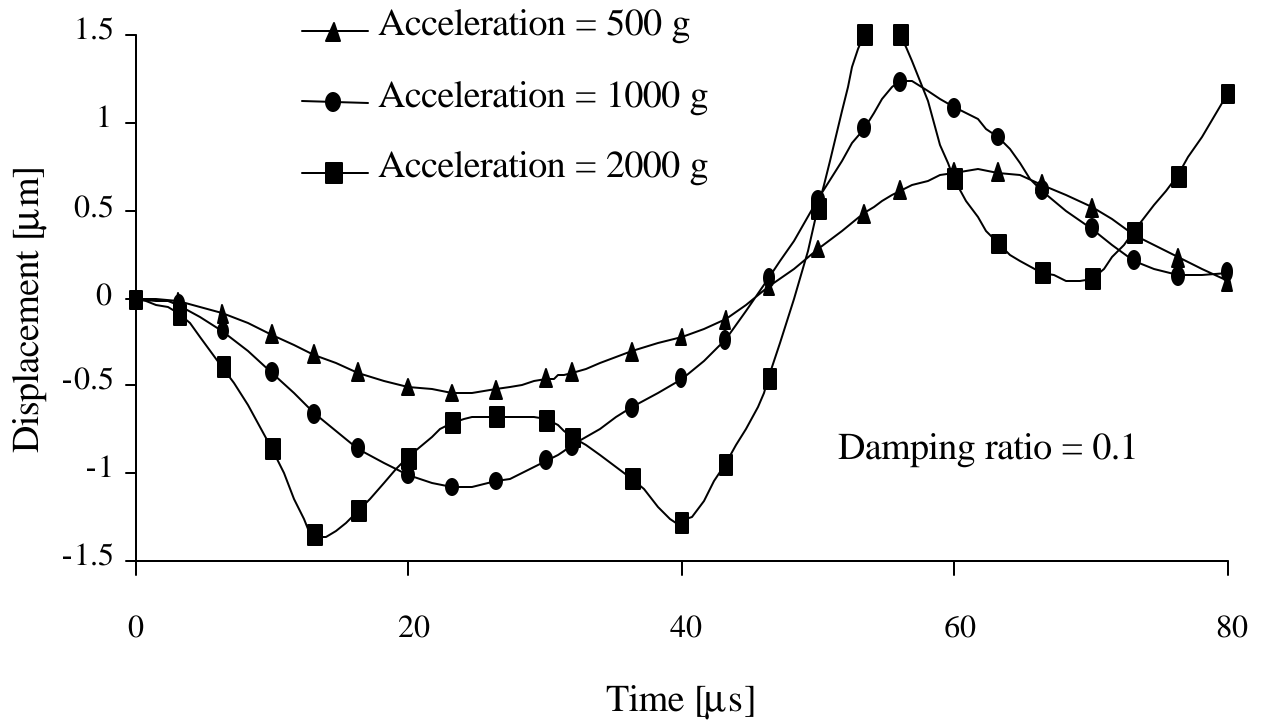

a) location at center

Figure 7 Transient curves of displacements for the transducer structure under high ‘g’

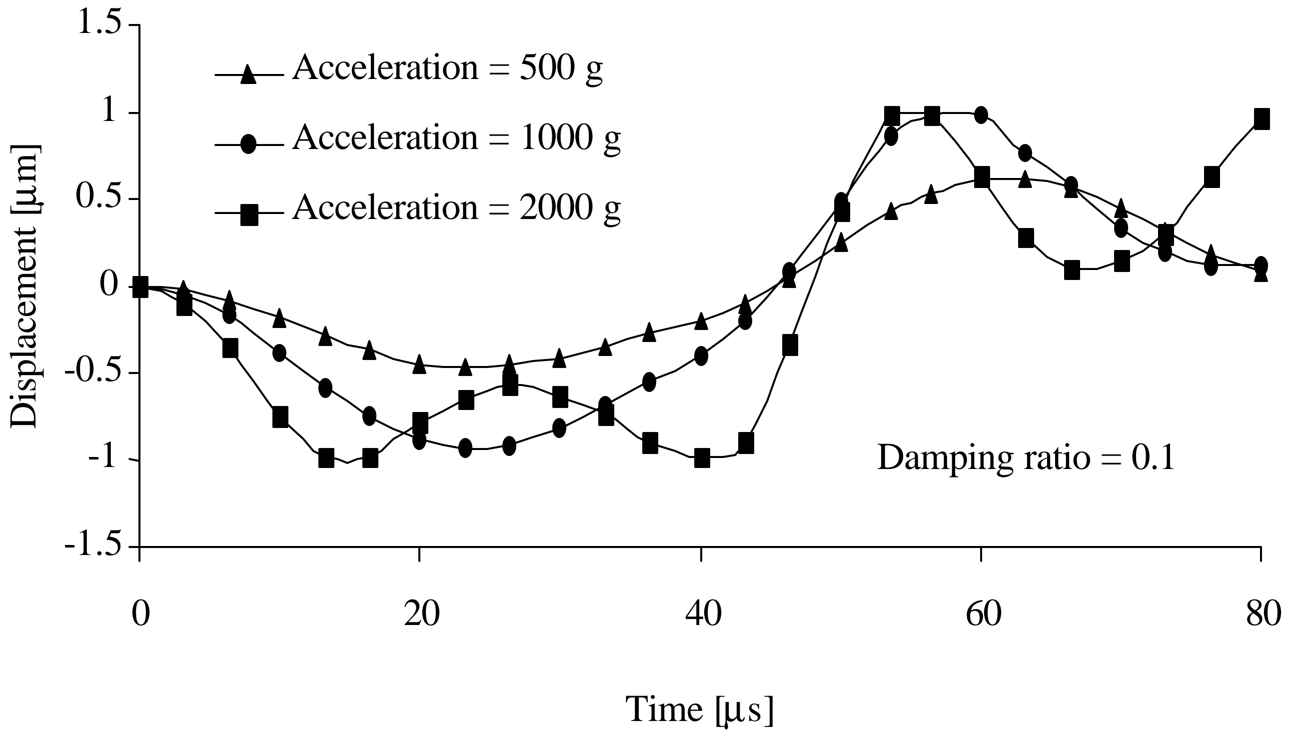

b) location at joint

Figure 7 Transient curves of displacements for the transducer structure under high ‘g’

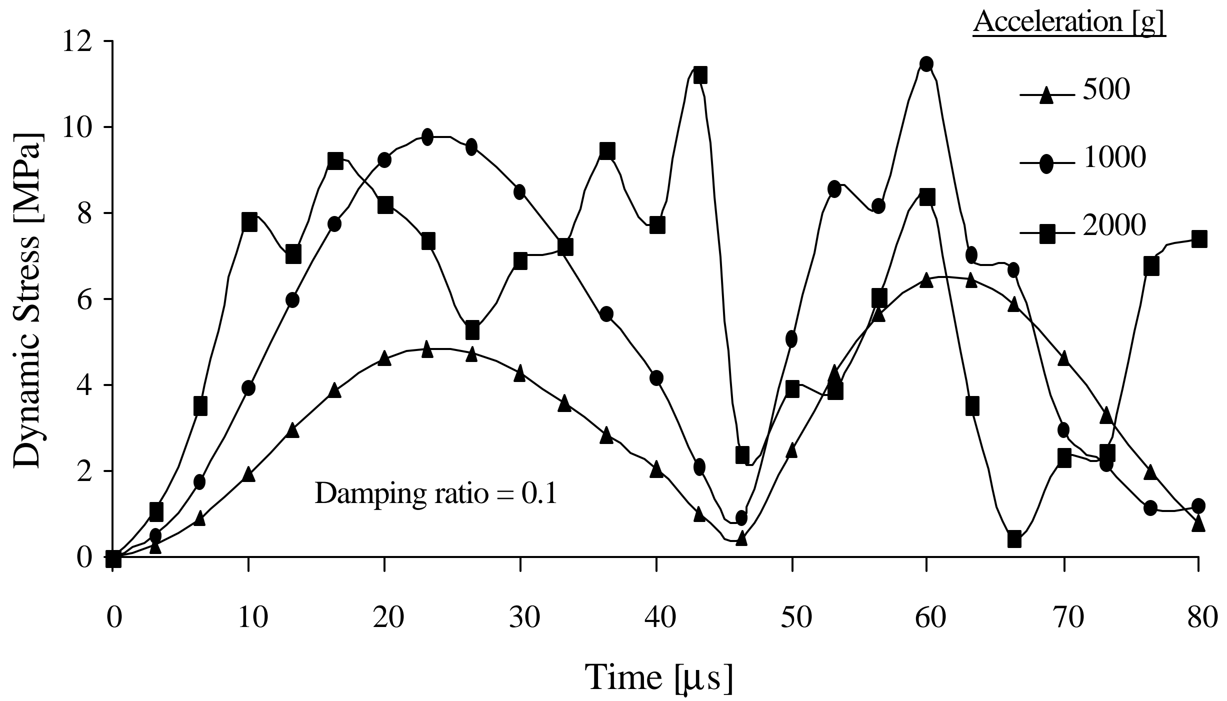

Figure 8 Dynamic stresses under high 'g'.

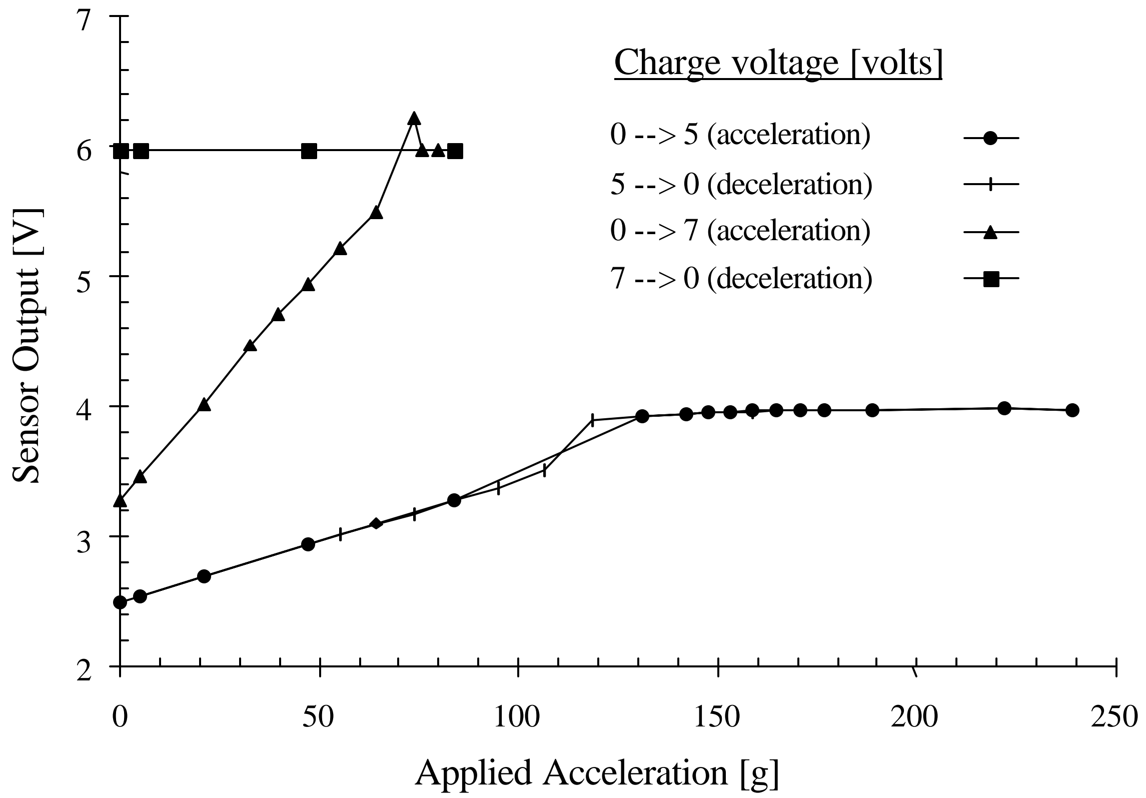

Figure 9 Latching test of accelerometer under two different operating voltages

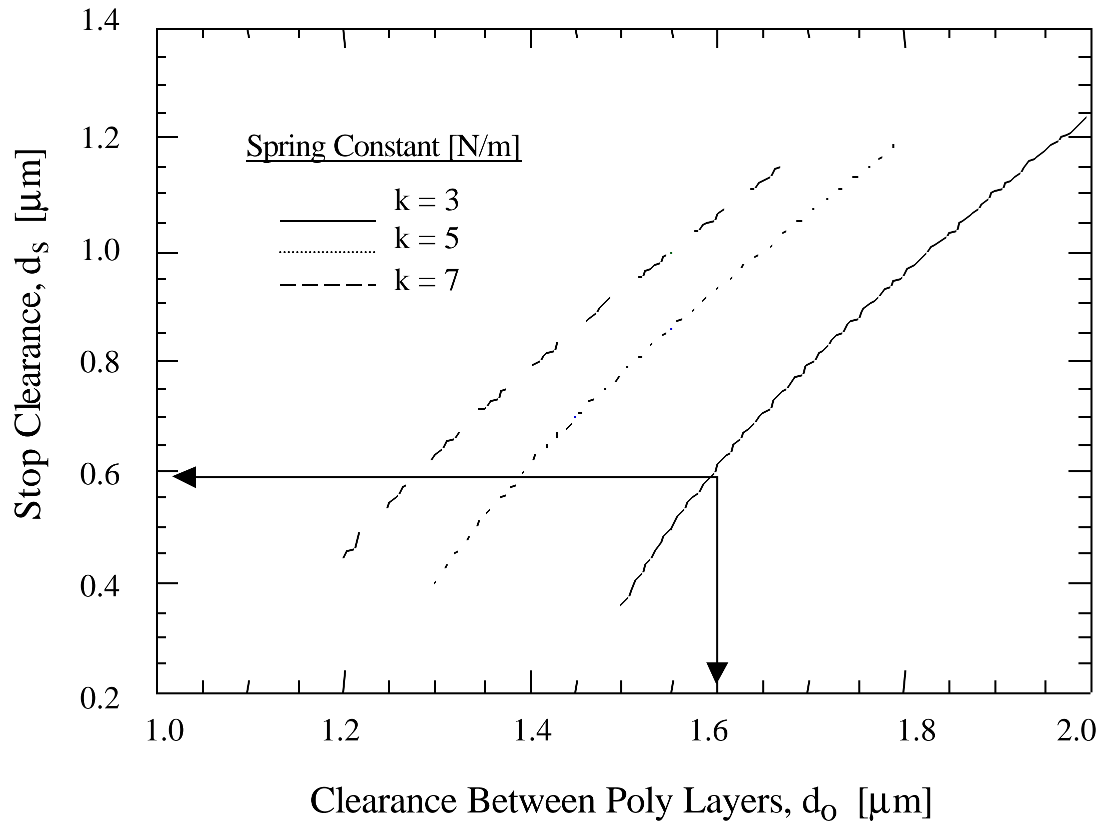

Figure 10: Latch criteria for a family of spring constants.

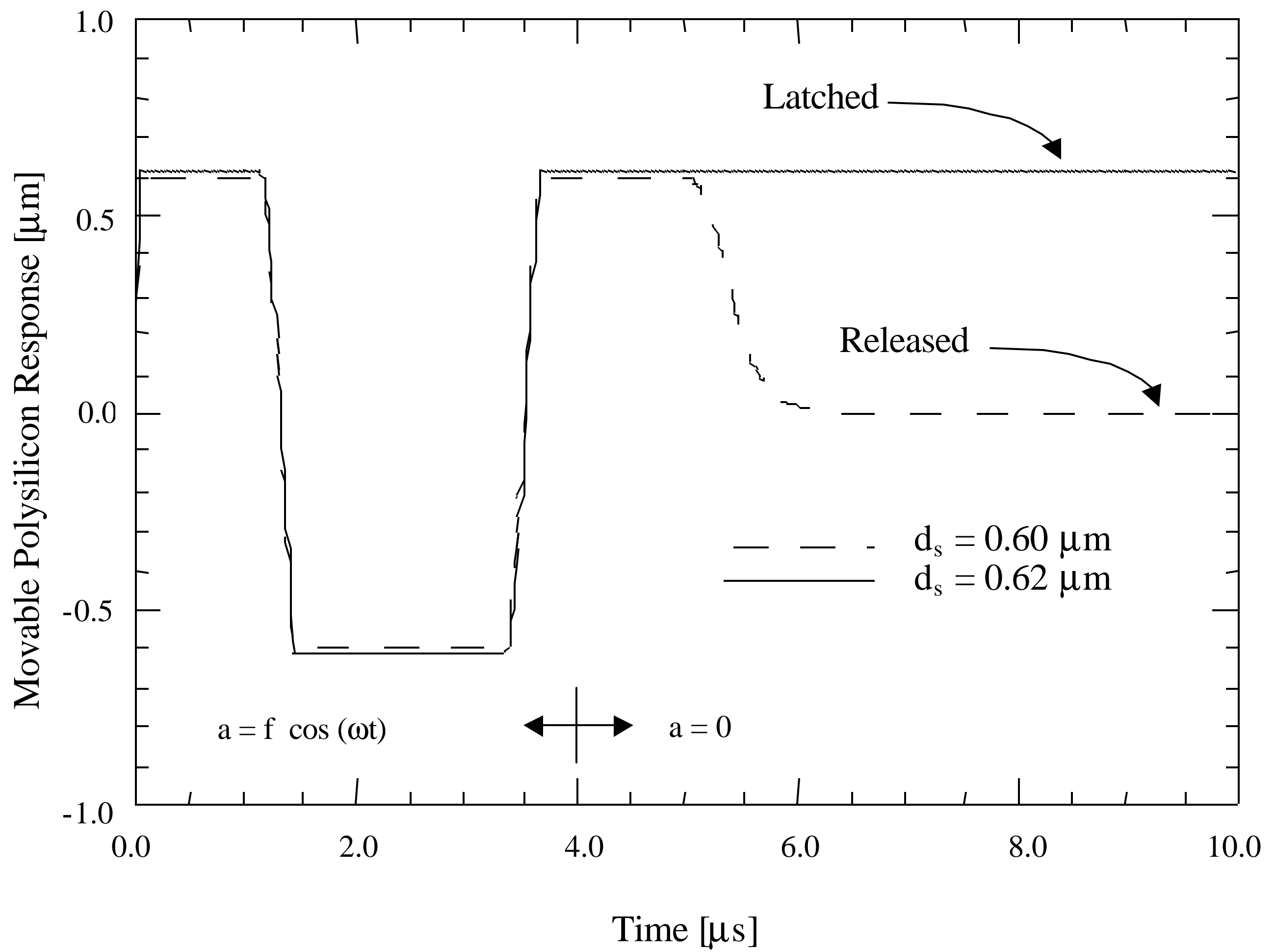

Figure 11 Numerical simulation of latch phenomenon